Supplemental Inventory

Figure S1 (related to Figures 1 and 2) - Sequence alignment of the PRFSTP motifs in HIM-8 and ZIMs in *Caenorhabditis* species and in vitro kinase assays verifying the activity of recombinant CHK-2

Figure S2 (related to Figures 2 and 3) - CHK-2 phosphorylation of HIM-8 and ZIMs occurs upon meiotic entry and persists until mid-pachytene

Figure S3 (related to Figures 2, 3, and 7) - Phosphorylation of the pairing center proteins is temporally correlated with chromosomal loading of DSB-1

Figure S4 (related to Figure 2) - Phosphorylation of HIM-8 T64 primes PLK-2 recruitment to the X chromosome pairing center

Figure S5 (related to Figure 3) – Phospho-HIM-8/ZIMs staining in different meiotic mutants.

Figure S6 (related to Figure 5) - Characterization of *C. elegans* strains expressing HTP-3 GK mutation series in four central closure motifs.

Figure S7 (related to Figure 6) - Characterization of *C. elegans* strains expressing HIM-3^{G280K} and/or HTP-3 transgenes carrying GK mutations in the closure motifs.

Supplemental Experimental Procedures

References

Supplemental Figure Legends

Figure S1 (Related to Figures 1 and 2). Sequence alignment of the PRFSTP motifs in HIM-8 and ZIMs in *Caenorhabditis* species

(A) *In vitro* kinase assays using wild-type and kinase-dead (K199R) CHK-2 expressed in insect cells and myelin basic protein as a positive control. Products were separated by SDS-PAGE. Gels were stained with Coomassie (left) and radiolabel incorporation was analyzed by autoradiography. (B) Sequence alignment of the N-terminal regions of all pairing center proteins in several *Caenorhabditis* species using the T-coffee algorithm. PRFSTP motifs for CHK-2 phosphorylation and PLK-2 docking and the putative binding motif for Chk2 FHA domain (pT-X-X-(L/I/M) (Li et al., 2002) are indicated.

Figure S2 (Related to Figures 2 and 3). CHK-2 phosphorylation of HIM-8 and ZIMs occurs upon meiotic entry and persists until mid-pachytene

(A) Immunofluorescence images of dissected gonad from wild-type hermaphrodites stained for DNA, HIM-8, pHIM-8/ZIMs, and SUN-1 pS12. The CHK-2 active zone is marked by dotted white lines. (Note: our pHIM-8/ZIMs antibody recognizes a CHK-2-independent epitope in mitotic nuclei) Scale bar, 50 μm. (B) Wild-type nuclei from different stages of meiotic prophase (transition zone, mid- and late-pachytene) were stained for DNA (blue), HIM-8 (red), pHIM-8/ZIMs (green), and SUN-1 pS12 (white). Meiotic entry in the transition zone was determined by DNA morphology and SUN-1 pS12 staining, and marked by a dotted line. Transition zone nuclei with paired or unpaired X chromosomes are highlighted with circles. Scale bar, 5 μm.

Figure S3 (Related to Figures 2, 3, and 7). Phosphorylation of the pairing center proteins is temporally correlated with chromosomal loading of DSB-1

(A-B) Dissected whole gonads from wild-type (A) and *syp-2* hermaphrodites (B) were stained for DNA, pHIM-8/ZIMs, and DSB-1. The CHK-2 active zone and DSB-1 zone are marked by yellow dotted lines. Scale bars, 50 μm.

Figure S4 (Related to Figure 2). Phosphorylation of HIM-8 T64 primes PLK-2 recruitment to the X chromosome pairing center

(A) Table showing the percent viable and male self-progeny from *C. elegans* hermaphrodites of indicated genotypes. (B) Immunofluorescence images of mid-pachytene nuclei stained for DNA (blue), HIM-8 (white), SYP-1 (red), and HTP-3 (green). (C) Projection images of transition zone nuclei from wild-type and *him-8*^{T64A} mutants stained for DNA (blue), HIM-8 (white), pHIM-8/ZIMs (green), and PLK-2 (red). Scale bars, 5 μm.

Figure S5 (Related to Figure 3). Phospho-HIM-8/ZIMs staining in different meiotic mutants.
(A-F) Germlines were dissected from *plk-2(tm1395); plk-1(RNAi)*, *him-8(tm611)*, *spo-11(me44)*, *zhp-3(jf61)*, *him-3(gk149)*, *and htp-1(gk174)* mutant strains and stained for DNA and pHIM-8/ZIMs. Note: our pHIM-8/ZIMs antibody recognizes a CHK-2 independent epitope in mitotic nuclei. The CHK-2 active zone is marked by dotted yellow lines. Scale bar, 50 μm.

Figure S6 (Related to Figure 5). Characterization of *C. elegans* strains expressing HTP-3 GK mutation series in four central closure motifs.
(A) Western blot showing the expression of HTP-3-GFP transgenes in the *htp-3(tm3655)* background. (B) Table showing the percent egg viability and male self-progeny from indicated genotypes. (C) Mid-pachytene nuclei of worm strains expressing wild-type and mutant HTP-3 transgenes in the *htp-3(tm3655)* background were stained for DNA, HTP-3 HTP-1, and HIM-3. All images are maximum-intensity projections of deconvolved 3D image tacks. Scale bar, 5 μm. (D) Mid-pachytene nuclei of the HTP-3^{3GK} strain were stained by immunofluorescence for DNA (white), HIM-8 (purple), HTP-3 (red), and SYP-1 (green). Scale bar, 5 μm.

Figure S7 (Related to Figure 6). Characterization of *C. elegans* strains expressing HIM-3 G280K and/or HTP-3 transgenes carrying mutations in closure motifs.
(A) Schematic of the GK mutations used in the study. (B) Sequence alignment of the closure motifs in HIM-3 and HTP-3 that bind HTP-1/2. To test the significance of HORMA domain:closure motif interaction between HTP-1/2 and HIM-3, the HIM-3^{G280K} mutation was introduced at the endogenous *him-3* locus by Cas9-CRISPR-mediated homologous recombination. (C) Untagged HTP-1 and wild-type or G280K mutant HIM-3-6His were co-expressed in *E. coli*, and protein complexes were purified using a His pulldown. Coomassie staining of SDS-PAGE shows the purified complexes. (D) Immunofluorescence images of dissected gonads from *syp-2; him-3*^{G280K} mutant strains stained for DNA

(blue) and pHIM-8/ZIMs (yellow). Scale bar, 50 μm. The HIM-3^{G280K} mutation did not fully suppress the extension of CHK-2 activity in *syp-2* mutants (76% in *syp-2; him-3^{G280K}*). Thus, while both HIM-3 and HTP-1/2 are essential for feedback regulation of CHK-2, their direct interaction through HORMA domain:closure motif binding is dispensable. (E) Table showing the percent egg viability and male self-progeny from indicated genotypes. (F) Mid-pachytene nuclei of worm strains expressing HIM-3^{G280K}, HIM-3^{G280K} and HTP-3$^{G490K, G728K}$, and HTP-3^{6GK} were stained for DNA, HTP-3, HTP-1, and HIM-3. Scale bar, 5 μm.

Supplemental Experimental Procedures

C. elegans strains

All strains were maintained at 20 °C under standard conditions. The wild-type strain was N2 Bristol. The following mutations and balancers were used: *htp-3(tm3655) I*, *him-3(gk149) IV, htp-1(gk174) IV*, *htp-2(tm2543) IV*, *him-8(tm611) IV*, *him-8(me4) IV*, *syp-2(ok307) V*, *spo-11(me44) IV*, *zhp-3(jf61) I*, *msh-5(me23) IV*, *him-5(ok1896) V*, *plk-2(tm1395) I*, *chk-2(me64) V,* and *ieDf2 IV*; *hT2 [bli-4(e937) let-?(q782) qIs48] (I;III), nT1[unc-?(n754) let-?(m435)] (IV;V), and mIs11[myo2p::GFP + pes-10p::GFP + gut-promoter::GFP]*.

Generation of *him-8*^{T64A} and *him-3*^{G280K} strains by Cas9/CRISPR-mediated homologous recombination

To generate *him-8*^{T64A}, Q5 site-directed mutagenesis was used to insert a Cas9 targeting sequence for *him-8* (ATTTACAGAATGAATTCGC) into pDD162 (Peft-3::Cas9 + empty sgRNA) (Dickinson et al., 2013) and to introduce silent mutations (ATTTACAGAACGAGTTTGC) into a repair template (pCFJ151 *him-8*^{T64A}). N2 worms were injected with Cas9 + *him-8* sgRNA construct (50 ng/µl), a repair template (50 ng/µl), pGH8 (10 ng/µl), pCFJ104 (5 ng/µl), and pCFJ90 (2.5 ng/µl). F_1 progeny were lysed and screened for homologous recombination by PCR using a forward primer specific to the endogenous *him-8* gene (TGAAGTTTAGTTTTCGCAGAATTCG) and a reverse primer specific to the mutated *him-8* Cas9 targeting sequence on the repair template (CTGCCACCCGCAAACTCG). Successful introduction of the T64A mutation at the endogenous *him-8* locus was verified by sequencing.

For *him-3*^{G280K}, Q5 site-directed mutagenesis was used to insert a Cas9 targeting sequence for *him-3* (CAAACCAATCGAAAAGGAA) into pDD162 (Peft-3::Cas9 + empty sgRNA) (Dickinson et al., 2013). Isothermal assembly with a synthetic gene block containing the G280K mutation and silent mutations in the Cas9 targeting sequence (CAAACCAAAGCAAGCGTAAA) was used to generate a repair template (pCFJ151 *him-3*^{G280K}). N2 worms were injected with Cas9 + *him-3* sg RNA construct (50 ng/µl), a repair template (50 ng/µl), pCFJ104 (5 ng/µl), and pCFJ90 (2.5 ng/µl). F_1 progeny were lysed and screened for homologous recombination by PCR using a forward primer specific to the endogenous *him-3* gene (CCACCGAAATCCACAATTTCTCG) and a reverse primer specific to the mutated *him-3* Cas9 targeting sequence on the repair template (GAAATTCGTCCTTTACGCTTGCT). The G280K mutation at the endogenous *him-3* locus was verified by sequencing. Both *him-8*^{T64A} and *him-3*^{G280K} strains were outcrossed three times before analysis.

Generation of transgenic worm strains by MosSCI

Strains carrying wild-type and mutant *htp-3-gfp* transgenes were generated by Mos1-mediated single copy insertion (MosSCI) (Frøkjaer-Jensen et al., 2008), as previously described (Kim et al., 2014). Briefly, pOR109, in which the *htp-3* genomic sequence fused to a GFP coding sequence was inserted into pCFJ151, was used to construct repair templates containing point mutations by Q5 mutagenesis (NEB) or isothermal assembly using synthetic gene fragments (IDT). Homozygous insertions at the ttTi5605 locus (Chr II) were verified by PCR, and crossed into *htp-3(tm3655)* to examine meiotic processes.

***plk-1* RNAi and egg count**

plk-1 RNAi was performed as described (Harper et al., 2011) using a RNAi clone from the Ahringer laboratory (Fraser et al., 2000; Harper et al., 2011). Briefly, L4 hermaphrodites were placed on RNAi plates, and animals were dissected for immunofluorescence analysis after 40 hours. Efficacy of *plk-1* RNAi was confirmed by the appearance of polyploid nuclei in the mitotic zone and embryonic arrest.

To score egg viability and male progeny, L4 hermaphrodites were picked onto individual plates and transferred to new plates every 12 hours for a total of 4-5 days. Eggs were counted immediately after removal of the parents, and surviving progeny were scored when the F_1 reached adulthood.

Immunofluorescence

Dissected gonads were fixed and stained for immunofluorescence according to standard protocols (Phillips et al., 2009). Briefly, adult hermaphrodites (24 hours post L4) were dissected in egg buffer (25 mM HEPES, pH 7.4, 118 mM NaCl, 48 mM KCl, 2 mM EDTA, 0.5 mM EGTA) containing 15 mM sodium azide and 0.1% Tween 20, and fixed with 1% formaldehyde in the same buffer between a Histobond slide (VWR) and a coverslip for 3 min. Slides were then frozen on dry ice or liquid nitrogen, and transferred to -20°C methanol after removing the coverslip. After 1 min, slides were washed with PBST (PBS containing 0.1% Tween 20) and blocked in blocking reagent (Roche) in PBST. Primary antibody incubations were conducted in blocking reagent for at least 2 hours at room temperature or overnight at 4°C. Primary antibodies were used at following concentrations: HIM-8 (rat, 1:300), HTP-1 (rabbit, 1:500), HTP-3 (guinea pig, 1:500), SYP-1 (goat, 1:500), phospho-HIM-8/ZIMs (rabbit, 1 μg/ml

of affinity purified antibody), PLK-2 (guinea pig, 1:300), SUN-1 pS12 (guinea pig, 1:300), and DSB-1 (guinea pig, 1:300). Secondary antibodies labeled with Alexa 488, Cy3, or Cy5 were purchased from Jackson ImmunoResearch. DNA was detected using 0.5 μg/ml DAPI and slides were mounted in Prolong Gold (Life Technologies). All images were acquired using either DeltaVision RT or Elite systems (Applied Precision) equipped with a 100X N.A. 1.4 oil-immersion objective (Olympus). Image deconvolution and projection were performed using the SoftWoRx Suite (Applied Precision).

References

Dickinson, D.J., Ward, J.D., Reiner, D.J., and Goldstein, B. (2013). Engineering the Caenorhabditis elegans genome using Cas9-triggered homologous recombination. Nature Methods *10*, 1028-1034.

Fraser, A.G., Kamath, R.S., Zipperlen, P., Martinez-Campos, M., Sohrmann, M., and Ahringer, J. (2000). Functional genomic analysis of C. elegans chromosome I by systematic RNA interference. Nature *408*, 325-330.

Harper, N.C., Rillo, R., Jover-Gil, S., Assaf, Z., Bhalla, N., and Dernburg, A.F. (2011). Pairing Centers Recruit a Polo-like Kinase to Orchestrate Meiotic Chromosome Dynamics in C. elegans. Developmental Cell *21*, 934-947.

Kim, Y., Rosenberg, S.C., Kugel, C.L., Kostow, N., Rog, O., Davydov, V., Su, T.Y., Dernburg, A.F., and Corbett, K.D. (2014). The Chromosome Axis Controls Meiotic Events through a Hierarchical Assembly of HORMA Domain Proteins. Developmental Cell *31*, 487-502.

Li, J., Williams, B.L., Haire, L.F., Goldberg, M., Wilker, E., Durocher, D., Yaffe, M.B., Jackson, S.P., and Smerdon, S.J. (2002). Structural and Functional Versatility of the FHA Domain in DNA-Damage Signaling by the Tumor Suppressor Kinase Chk2. Molecular Cell *9*, 1045-1054.

Phillips, C.M., McDonald, K.L., and Dernburg, A.F. (2009). Cytological Analysis of Meiosis in Caenorhabditis elegans. Methods in Molecular Biology *558*, 171-195.

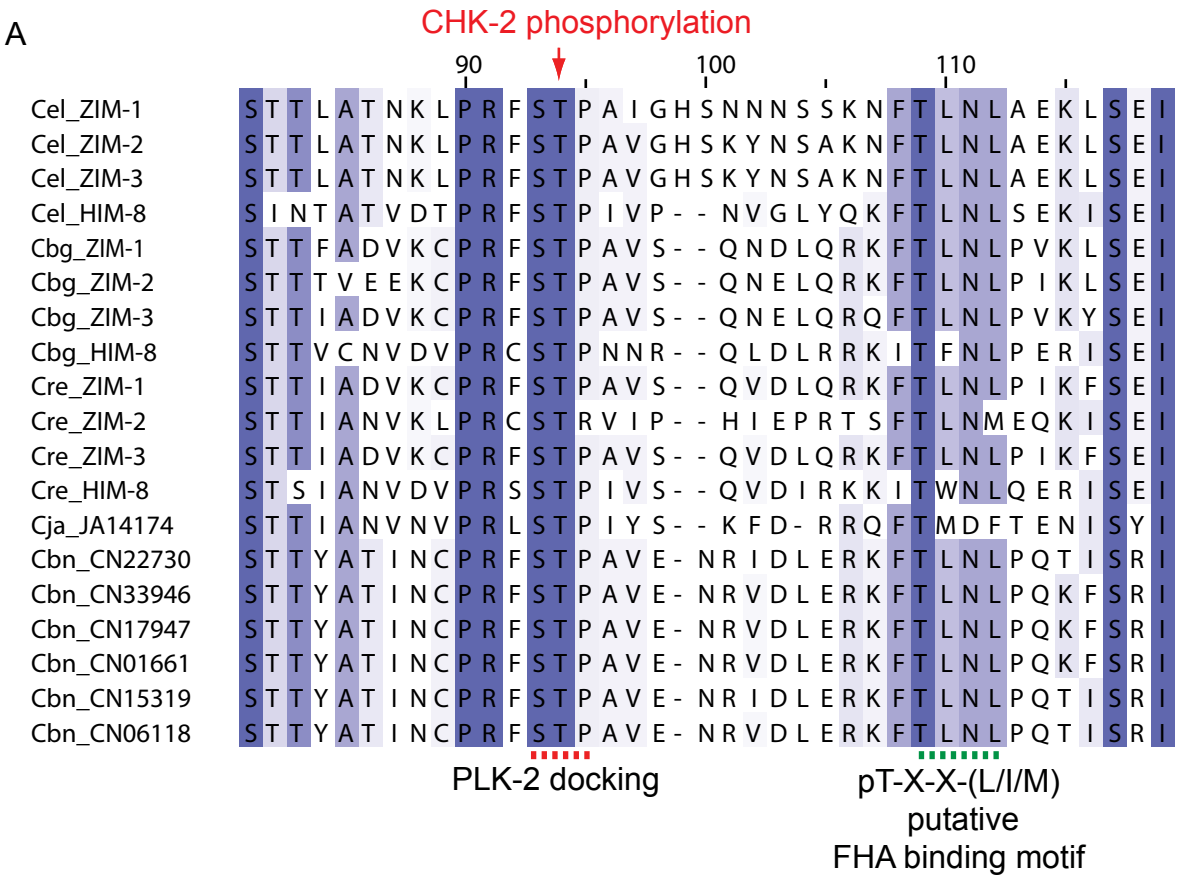
A
CHK-2 phosphorylation
90
100
110
Cel_ZIM-1 S T T L A T N K L P R F S T P A I G H S N N N S S K N F T L N L A E K L S E I
Cel_ZIM-2 S T T L A T N K L P R F S T P A V G H S K Y N S A K N F T L N L A E K L S E I
Cel_ZIM-3 S T T L A T N K L P R F S T P A V G H S K Y N S A K N F T L N L A E K L S E I
Cel_HIM-8 S I N T A T V D T P R F S T P I V P - - N V G L Y Q K F T L N L S E K I S E I
Cbg_ZIM-1 S T T F A D V K C P R F S T P A V S - - Q N D L Q R K F T L N L P V K L S E I
Cbg_ZIM-2 S T T T V E E K C P R F S T P A V S - - Q N E L Q R K F T L N L P I K L S E I
Cbg_ZIM-3 S T T I A D V K C P R F S T P A V S - - Q N E L Q R Q F T L N L P V K Y S E I
Cbg_HIM-8 S T T V C N V D V P R C S T P N N R - - Q L D L R R K I T F N L P E R I S E I
Cre_ZIM-1 S T T I A D V K C P R F S T P A V S - - Q V D L Q R K F T L N L P I K F S E I
Cre_ZIM-2 S T T I A N V K L P R C S T R V I P - - H I E P R T S F T L N M E Q K I S E I
Cre_ZIM-3 S T T I A D V K C P R F S T P A V S - - Q V D L Q R K F T L N L P I K F S E I
Cre_HIM-8 S T S I A N V D V P R S S T P I V S - - Q V D I R K K I T W N L Q E R I S E I
Cja_JA14174 S T T I A N V N V P R L S T P I Y S - - K F D - R R Q F T M D F T E N I S Y I
Cbn_CN22730 S T T Y A T I N C P R F S T P A V E - N R I D L E R K F T L N L P Q T I S R I
Cbn_CN33946 S T T Y A T I N C P R F S T P A V E - N R V D L E R K F T L N L P Q K F S R I
Cbn_CN17947 S T T Y A T I N C P R F S T P A V E - N R V D L E R K F T L N L P Q K F S R I
Cbn_CN01661 S T T Y A T I N C P R F S T P A V E - N R V D L E R K F T L N L P Q K F S R I
Cbn_CN15319 S T T Y A T I N C P R F S T P A V E - N R I D L E R K F T L N L P Q T I S R I
Cbn_CN06118 S T T Y A T I N C P R F S T P A V E - N R V D L E R K F T L N L P Q T I S R I
PLK-2 docking
pT-X-X-(L/I/M)
putative
FHA binding motif

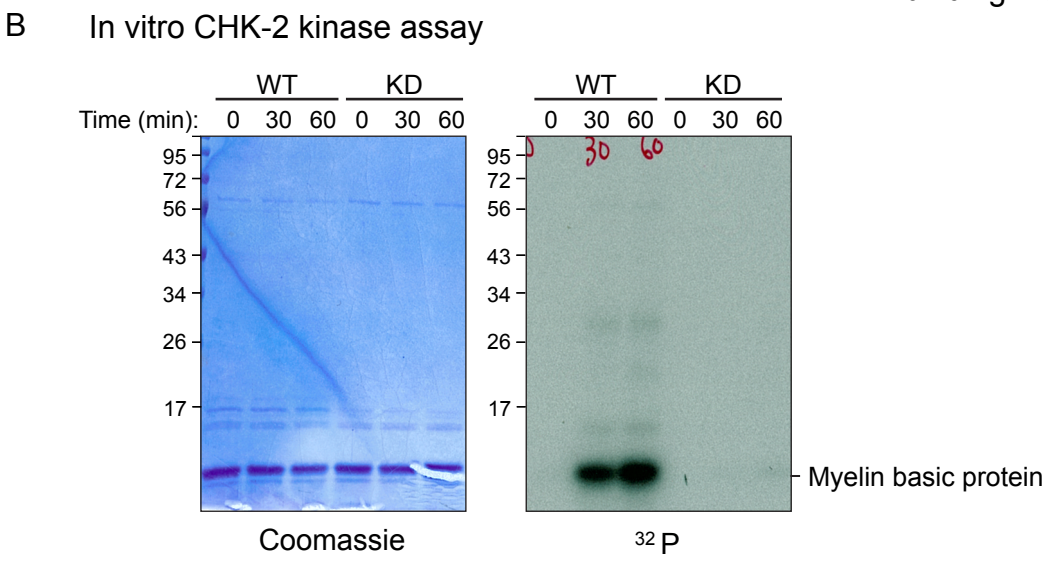
B
In vitro CHK-2 kinase assay
WT
KD
WT
KD
Time (min): 0 30 60 0 30 60
0 30 60 0 30 60
95
72
56
43
34
26
17
95
72
56
43
34
26
17
Myelin basic protein
Coomassie
32 P

Figure S1

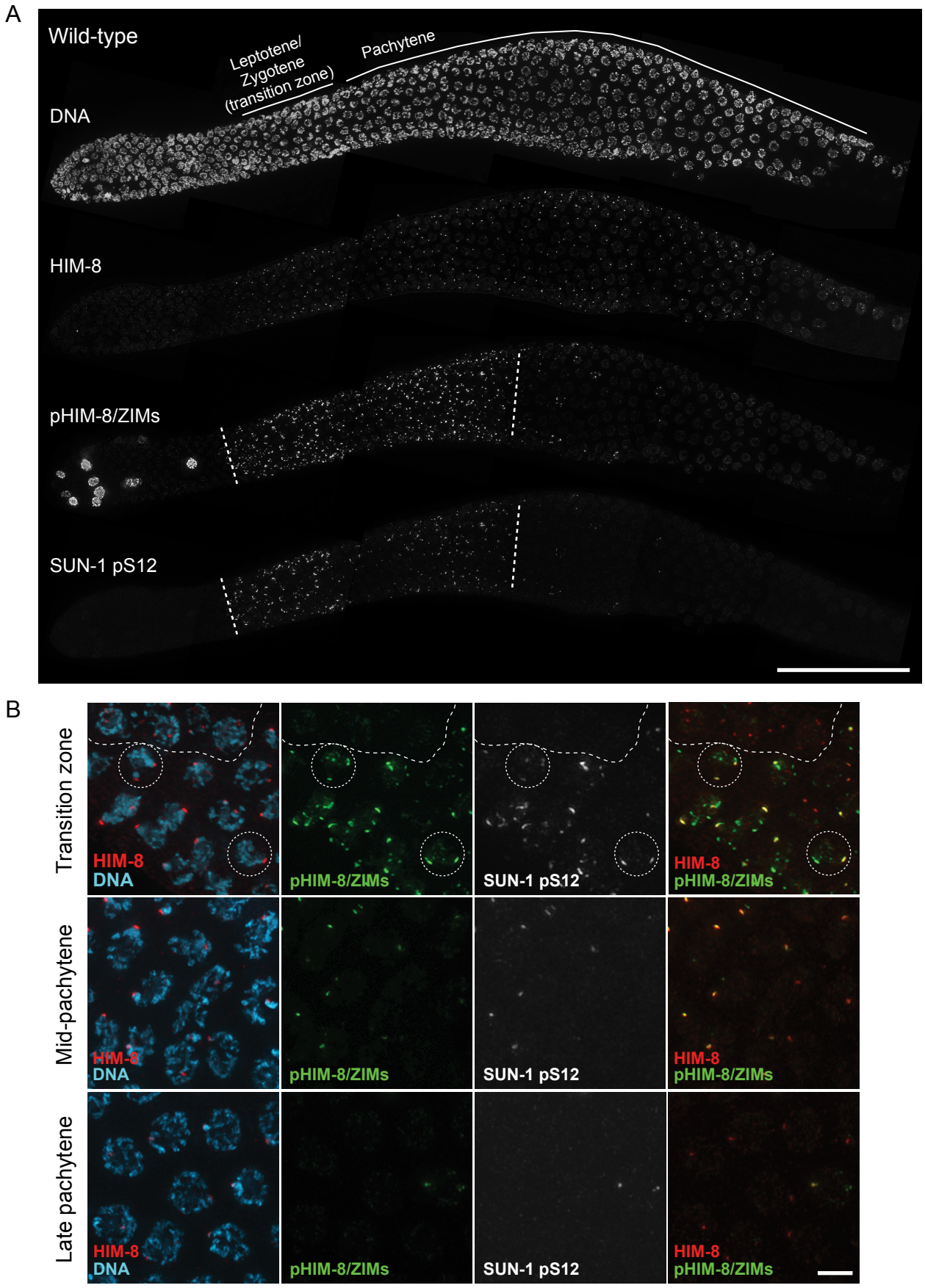
A
Wild-type
Leptotene/
Zygotene
(transition zone)
Pachytene
DNA
HIM-8
pHIM-8/ZIMs
SUN-1 pS12
B
Transition zone
Mid-pachytene
Late pachytene
HIM-8
DNA
pHIM-8/ZIMs
SUN-1 pS12
HIM-8
pHIM-8/ZIMs

Figure S2

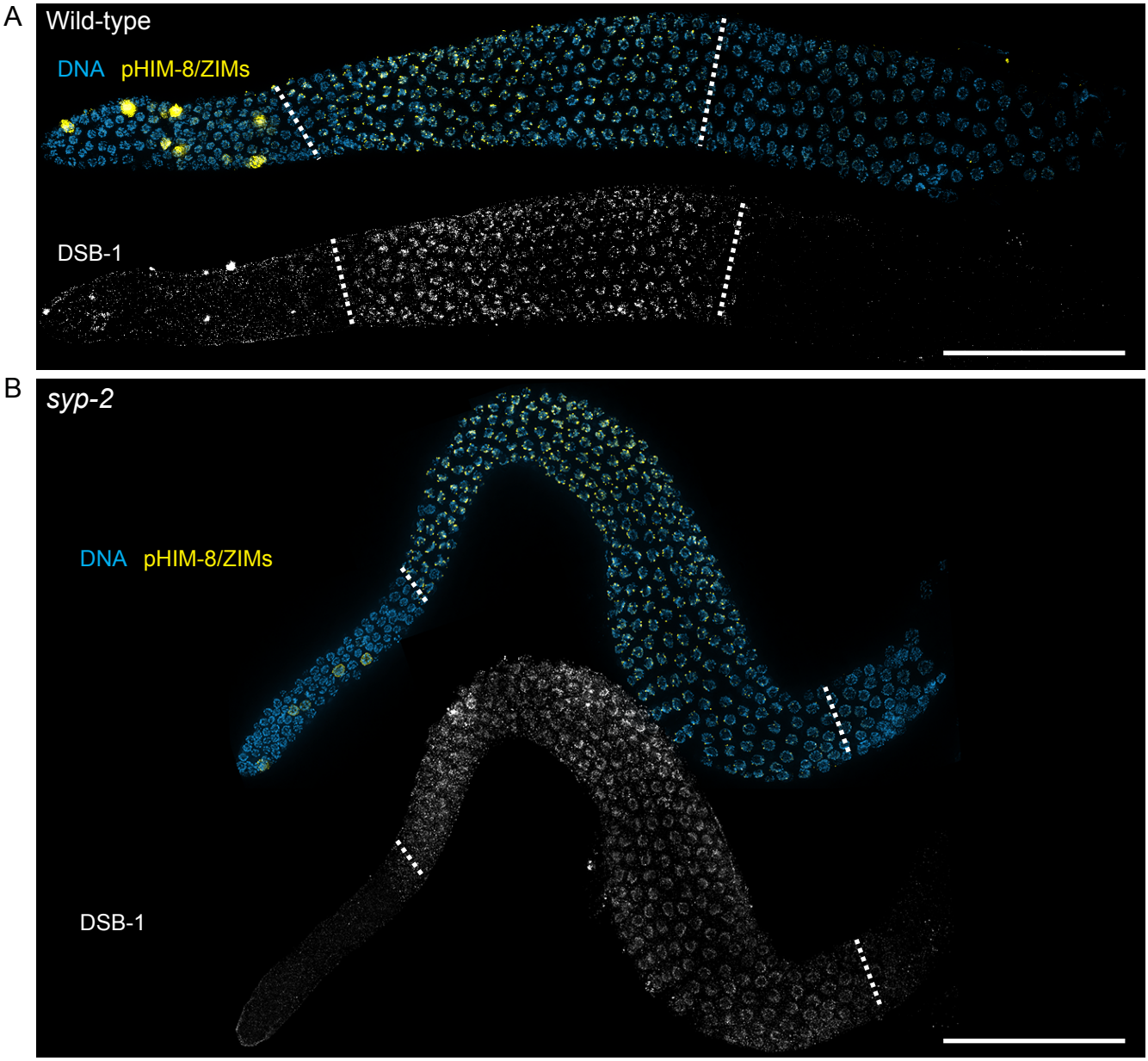

Figure S3

A

	% Viability (n)	% Males (n)
Wild-type	100 (438)	0.2 (1)
him-8(tm611)	99 (1120)	39 (429)
him-8^{T64A}	99 (1062)	41 (434)

B

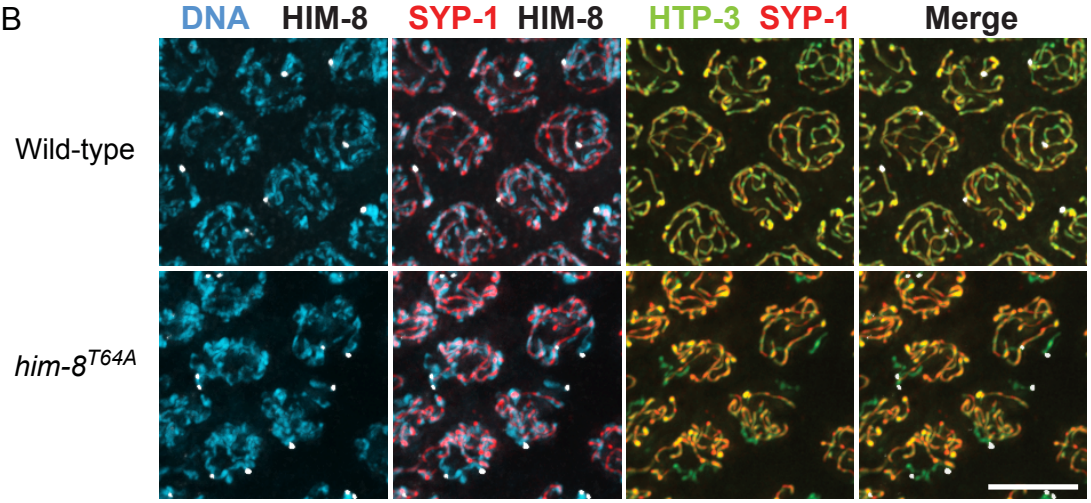

C

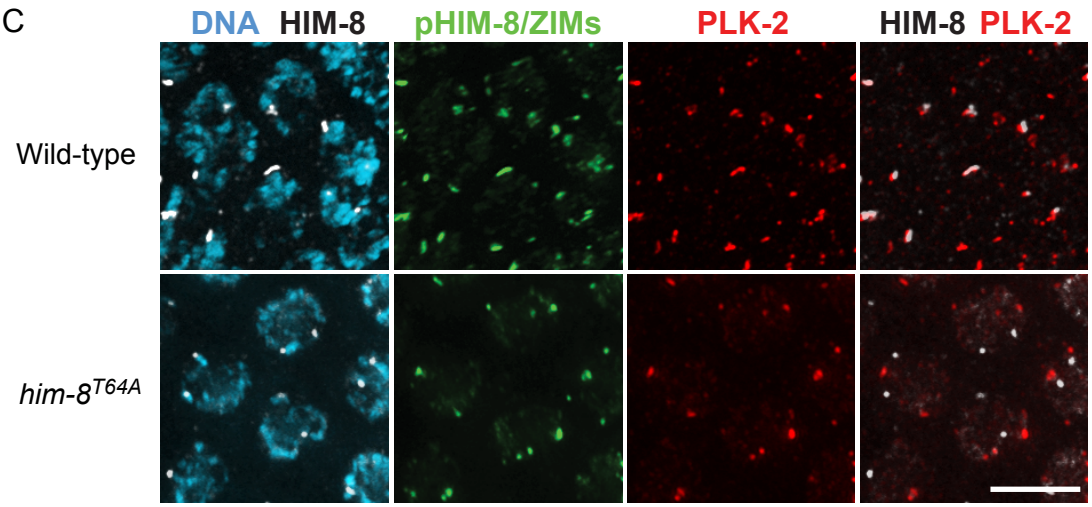

Figure S4

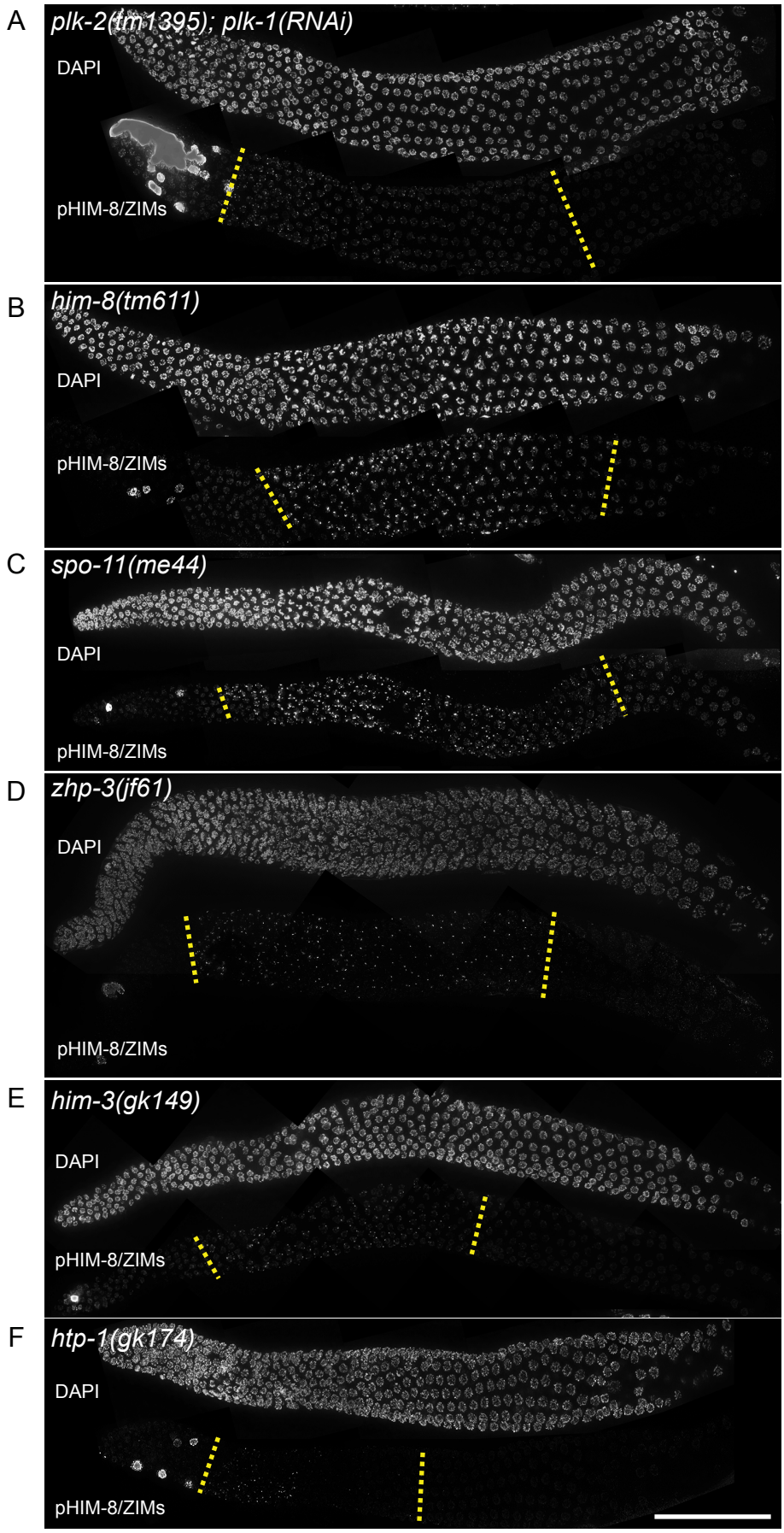
A
plk-2(tm1395); plk-1(RNAi)
DAPI
pHIM-8/ZIMs
B
him-8(tm611)
DAPI
pHIM-8/ZIMs
C
spo-11(me44)
DAPI
pHIM-8/ZIMs
D
zhp-3(jf61)
DAPI
pHIM-8/ZIMs
E
him-3(gk149)
DAPI
pHIM-8/ZIMs
F
htp-1(gk174)
DAPI
pHIM-8/ZIMs

Figure S5

A

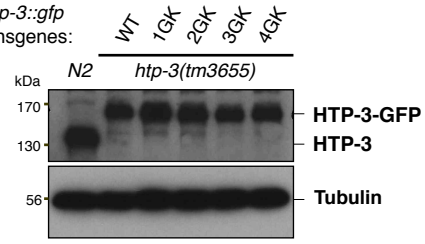

B

Genotypes	Egg viability (%)	Males (%)	Number of eggs
htp-3(tm3655) I	13	23.7	878
htp-3(tm3655) I; htp-3^{WT} *II*	100	0.28	679
htp-3(tm3655) I; htp-3^{1GK} *II*	79.2	1.5	1160
htp-3(tm3655) I; htp-3^{2GK} *II*	57.5	3.9	797
htp-3(tm3655) I; htp-3^{3GK} *II*	21.2	12.4	1143
htp-3(tm3655) I; htp-3^{4GK} *II*	3.1	27.5	1308

C

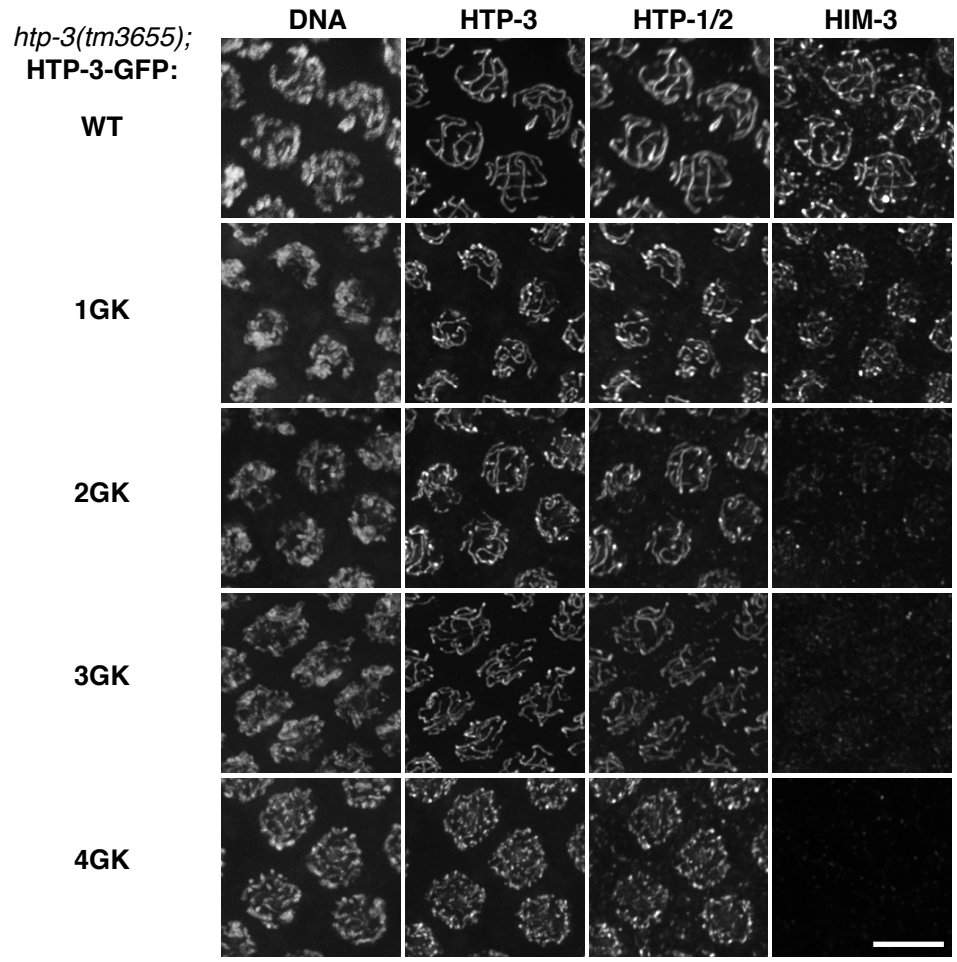

D

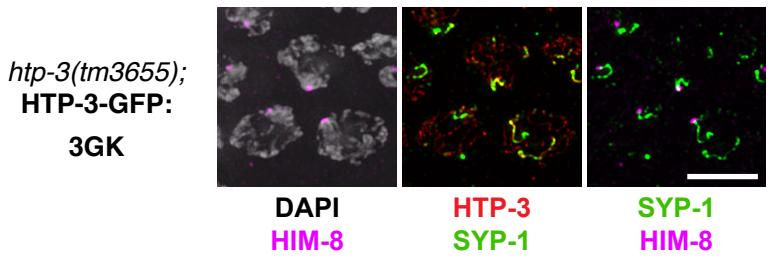

Figure S6

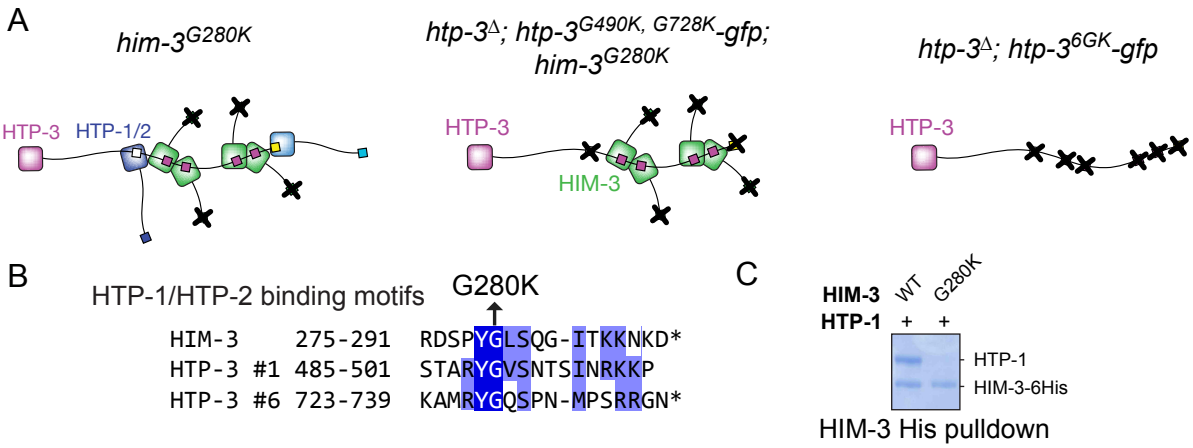

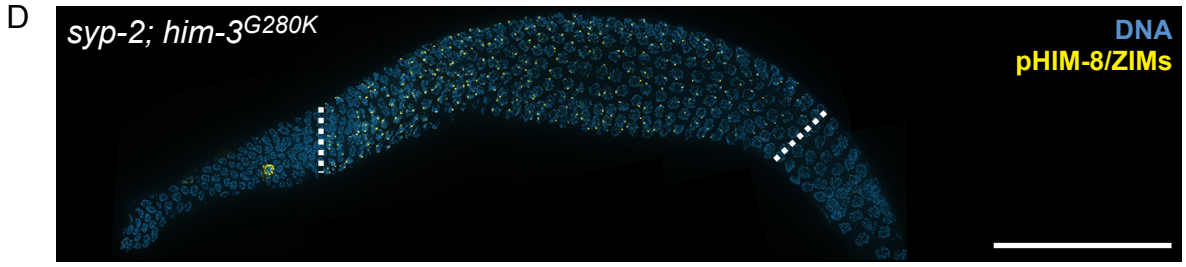

E

Genotypes	Egg viability (%)	Males (%)	Number of eggs
him-3^{G280K} IV	98	0.5	1231
htp-3(tm3655) I; htp-3$^{G490K, G728K}$-gfp II; him-3^{G280K} IV	17.4	15.1	1292
htp-3(tm3655) I; htp-3^{6GK}-gfp II	2	29.2	1226

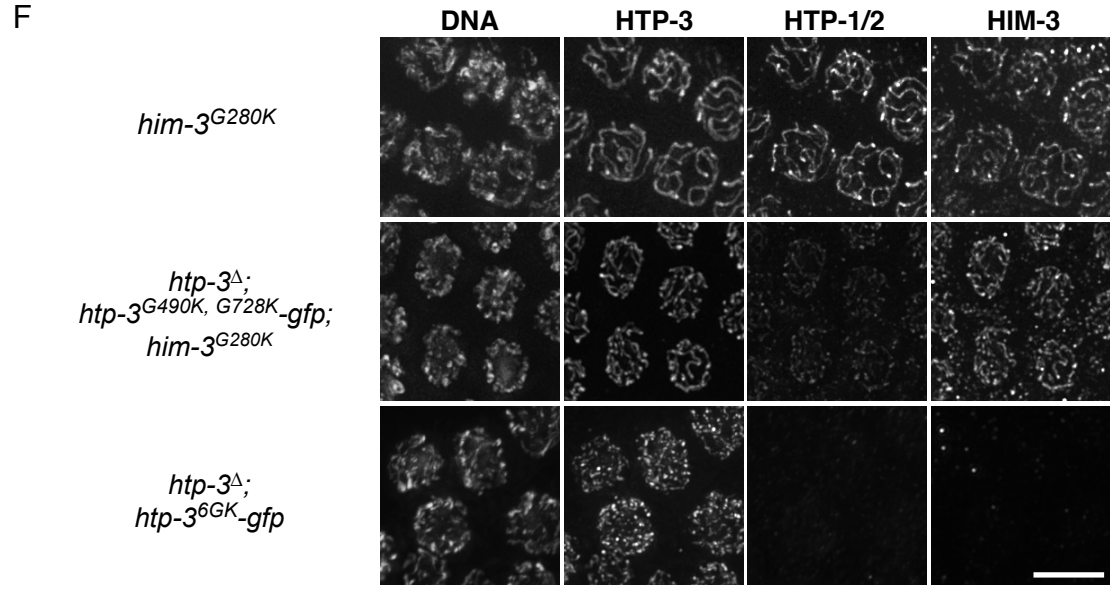

Figure S7